Elsevier Editorial System(tm) for Carbohydrate Polymers

Manuscript Draft

Manuscript Number: CARBPOL-D-15-03162R1

Title: Microfibrillated cellulose and borax as mechanical, O2-barrier, and surface-modulating agents of pullulan bionanocomposite coatings on BOPP

Article Type: Research Paper

Keywords: contact angle; food packaging; nanocomposite coatings; oxygen permeability

Corresponding Author: Dr. Stefano Farris,

Corresponding Author's Institution: University of Milan

First Author: Carlo A Cozzolino

Order of Authors: Carlo A Cozzolino; Gaetano Campanella; Hasan Türe; Richard T Olsson, Professor; Stefano Farris

Abstract: Multifunctional composite coatings on bi-oriented polypropylene (BOPP) films were obtained using borax and microfibrillated cellulose (MFC) added to the main pullulan coating polymer. Spectroscopy analyses suggested that a first type of interaction occurred via hydrogen bonding between the C6–OH group of pullulan and the hydroxyl groups of boric acid, while monodiol and didiol complexation represented a second mechanism. The deposition of the coatings yielded an increase in the elastic modulus of the entire plastic substrate (from ~2 GPa of the neat BOPP to ~ 3.1 GPa of the P/B+/MFC-coated BOPP). The addition of MFC yielded a decrease of both static and kinetic coefficients of friction of approximately 22% and 25%, respectively, as compared to the neat BOPP. All composite coatings dramatically increased the oxygen barrier performance of BOPP, especially under dry conditions. The deposition of the high hydrophilic coatings allowed to obtain highly wettable surfaces (water contact angle of ~18°).

Highlights (for review)

- We produce bionanocomposite coatings using pullulan, borax, and MFC
- We use the coatings as thin layers laid on BOPP films
- We evaluate mechanical, barrier, and surface properties of the coated films
- Adding borax and MFC will increase elastic modulus, oxygen-barrier, and wettability
- Pullulan/borax/MFC coatings show promising properties for food packaging applications

UNIVERSITÀ DEGLI STUDI DI MILANO
Department of Food, Environmental and Nutritional Sciences
Dipartimento di Scienze per gli Alimenti, la Nutrizione e l'Ambiente
DeFENS

Response to Reviewers

Dear Editor,

We would like to thank the Editorial team for fast handling of the manuscript and the reviewers for their valuable comments on our work. Their suggestions were used to improve the final form of the manuscript. Please find below a detailed list of changes that we have made on the previous version, according to the reviewers' reports. Answers to the reviewers' comments are in red.

Best regards,

Stefano Farris (on behalf of all authors)

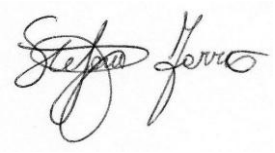

--
Stefano Farris, Ph.D. | PackLAB team
University of Milan
DeFENS, Department of Food, Environmental and Nutritional Sciences
PackLAB – Food Packaging Laboratory
via Celoria, 2 - 20133 MILANO
OFFICE +39 0250316654 | FAX +39 0250316672

Reviewers' comments:

Reviewer #1: Minor Revisions for acceptance

This paper presents a bionanocomposite coatings using pullulan, borax, and MFC aiming to improve the oxygen and water barrier, mechanical, optical, and surface properties of a BOPP film, a commonly-used plastic for food packaging applications.

The manuscript is well written. We regret that the authors didn't show the SEM-FEG images of the cross-section films prepared to check the adequate coverage of the surface with different coating. Indeed, a good coverage is required to develop a barrier layer.

We are thankful with the reviewer for his comments on our work. We have now added an experimental part including FE-SEM analyses of both surface and cross-section of pullulan-

Microfibrillated cellulose and borax as mechanical, O_2-barrier, and surface–modulating agents of pullulan biocomposite coatings on BOPP

Carlo A. Cozzolino[a], Gaetano Campanella[a], Hasan Türe[b], Richard T. Olsson[c], Stefano Farris[a]*

[a]*DeFENS, Department of Food, Environmental and Nutritional Sciences—Packaging Division, University of Milan, Milan, Italy*

[b]*Fatsa Faculty of Marine Science, Department of Marine Science and Technology Engineering, Ordu University, Ordu, Turkey*

[c]*Department of Fibre and Polymer Technology, School of Chemical Science and Engineering, KTH Royal Institute of Technology, Stockholm, Sweden*

*Corresponding author. Tel.: +39 0250316654; Fax: +39 0250316672

E-mail address: stefano.farris@unimi.it (S. Farris)

ABSTRACT

Multifunctional composite coatings on bi-oriented polypropylene (BOPP) films were obtained using borax and microfibrillated cellulose (MFC) added to the main pullulan coating polymer. Spectroscopy analyses suggested that a first type of interaction occurred via hydrogen bonding between the C_6−OH group of pullulan and the hydroxyl groups of boric acid, while monodiol and didiol complexation represented a second mechanism. The deposition of the coatings yielded an increase in the elastic modulus of the entire plastic substrate (from ~2 GPa of the neat BOPP to ~ 3.1 GPa of the P/B+/MFC-coated BOPP). The addition of MFC yielded a decrease of both static and kinetic coefficients of friction of approximately 22% and 25%, respectively, as compared to the neat BOPP. All composite coatings dramatically increased the oxygen barrier performance of BOPP, especially under dry conditions. The deposition of the high hydrophilic coatings allowed to obtain highly wettable surfaces (water contact angle of ~18°).

Keywords: contact angle; food packaging; composite coatings; oxygen permeability

Chemical compounds studied in this article

Pullulan (PubChem CID: 92024139); Borax (PubChem CID: 10219853)

1. Introduction

The use of biopolymers represents one of the most promising strategies towards an optimized use of conventional nonbiodegradable petroleum-based plastic packaging materials due to both lower environmental impact and improved technical performance (Barlow & Morgan, 2013; Rhim, Park, & Ha, 2013). Especially within the food packaging sector, the deposition of high performance biopolymer coatings on plastic films has been proposed as a possible first step toward the environmental and functional goals (Farris, Introzzi & Piergiovanni, 2009). According to the "packaging optimization" principle, the use of high-performance thin layers would allow down-gauging current packaging structures, e.g., laminates and/or co-extruded materials, without impairing (and, in fact, improving) the overall performance of the substrate beneath, at reasonable cost (Farris et al., 2014a).

Pullulan (Figure 1a) has attracted much attention over recent years as potential food packaging material due to its peculiar characteristics. This non-ionic exopolysaccharide is obtained from the fermentation medium of the black yeast *Aureobasidium pullulans* (originally called *Pullularia pullulans*) under limiting conditions (e.g., nitrogen), with media composition and culture conditions highly affecting the final yield. Dry pullulan is white, nontoxic, tasteless, odorless and biodegradable, with high film forming abilities (Yuen, 1974; Trovatti et al., 2012). The α–(1→6) linkage between maltotriose residues contributes to the structural flexibility and high solubility of pullulan (Leathers, 2003), whereas the presence of hydroxyl groups on the molecular skeleton is responsible for the extensive inter-molecular hydrogen bonding and super-hydrophilicity, which have been profitably exploited to develop an oxygen barrier and anti-fog coatings, respectively (Farris et al., 2012; Introzzi et al., 2012a).

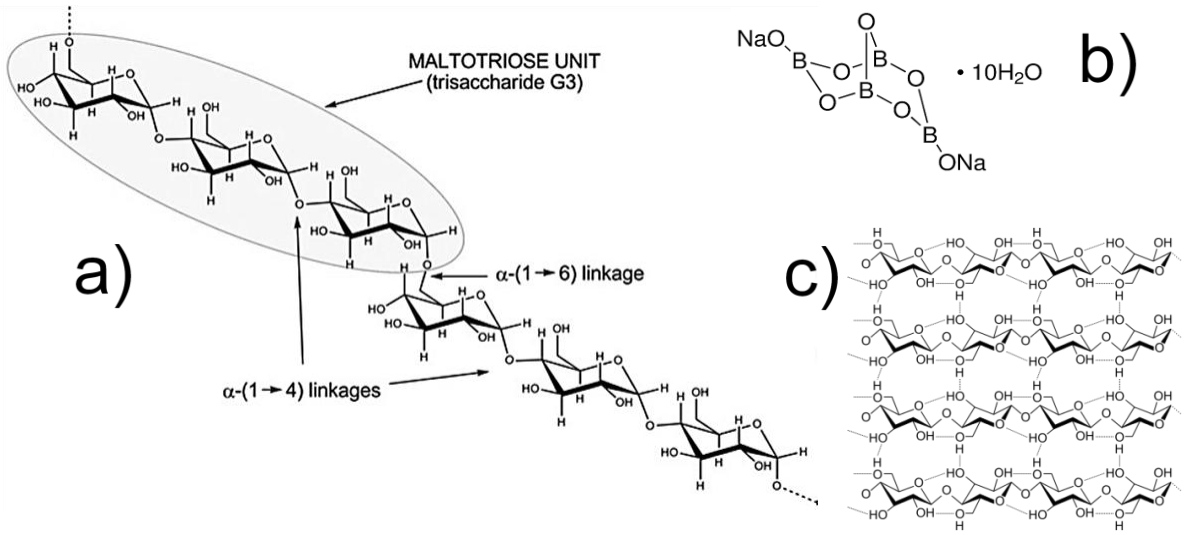

Figure 1. a) pullulan molecule as a sequence of repeating units of maltotriose (adapted from Farris et al., 2014); b) sodium tetraborate decahydrate; c) structure of cellulose (four molecular chains to form a strand) with intra- and inter-molecular hydrogen bonds (dashed lines) in evidence.

Another important feature of pullulan is its high transparency in the form of a thin layer, which is a sought-after property for all those applications envisaging adequate display (e.g., food packaging, optical devices, and monitors) (Introzzi et al., 2012a). Like most biopolymers, pullulan suffers some drawbacks, such as the sensitivity to moisture that dramatically affects its performance. Blending pullulan with other (bio)polymers has been shown as a valid strategy to control moisture sensitivity (Kristo & Biliaderis, 2007; Xiao, Lim & Tong, 2012; Wu et al., 2013). More recently, pullulan has been used in combination with natural montmorillonite (Na^+-MMT) (Introzzi et al., 2012b) and graphene (Unalan et al., 2015) to produce bionanocomposite materials with enhanced properties even at high relative humidity values intended for food packaging applications.

Borax (Figure 1b) is a salt of boric acid also known as sodium borate, sodium tetraborate, or disodium tetraborate. This water-soluble white powder is listed among the substances that can be used to produce plastic materials intended to come into contact with food (Annex I, Table 1, identification number 584 of EU Reg. 10/2011), with a specific migration limit of 6 mg kg^{-1} expressed as boron (Annex I, Table 2, group restriction number 16 of EU Reg. 10/2011). Recently the use of borax has been questioned due to its potential adverse effects on human health (genotoxicity). In 2013, the EFSA Panel on Food Additives and Nutrient Sources added to Food (ANS) provided a scientific opinion re-evaluating the safety of borax and boric acid as food additives (E 285 and E284, respectively) in the EU. Exposure estimates to boron from its use as food additive at the highest 95th percentile for consumers only, for children, adolescents, adults and the elderly would be 0.56, 0.37, 0.13 and 0.15 mg/kg bw/day, respectively. The Panel concluded that it is unlikely that a regular exceedance of the admitted daily intake (ADI) occurs (EFSA ANS, 2013). Borax finds a variety of applications as an additive of detergents and cosmetics, to make buffer solutions, as a fire retardant, and as a texturing agent and antimicrobial agent in the food industry (Yanjuan, Yanxiong, Wei & Chunying, 2013). Borax dissociates completely into equal quantities of trigonal planar [boric acid, $B(OH_3)$] and tetrahedral [monoborate ions, $2B(OH)_4^-$] that interchange rapidly in water system according to (Han, Lei & Wu, 2014):

$$Na_2B_4O_7 + 7H_2O = 2B(OH_3) + 2B(OH)_4^- \qquad \text{(reaction 1)}$$

The co-existence of both forms can be exploited profitably to generate water-based systems with enhanced hydrogen bonding (due to the hydroxyl groups) while preserving long-term stability (due to the hydroxide ions). Borax has desirable properties as a component of polymeric

84 composites because polar −OH groups facilitate strong interactions and mechanical stability
85 (Yunus, Unal, Erol & Sari, 2011).

86 Cellulose (Figure 1c) is a widely available, low cost, renewable, and biodegradable polymer.
87 Its chemical structure and physical properties have been widely reported in the literature
88 (Berglund, 2006; Cabiaca et al., 2011). Cellulose is mostly obtained from wood and cotton,
89 although cellulose pulp can be also extracted from agricultural byproducts such as bagasse, stalks
90 and crop straws and is also produced by many species of bacteria (e.g., *Gluconacetobacter spp.*)
91 (Huang et al., 2014). Cellulose fibers can be disassembled into their structural nano-components
92 (Chinga-Carrasco et al., 2011)—cellulose nanoparticles (CNs), such as microfibrillated cellulose
93 (MFC; or cellulose microfibrils, CMF); cellulose nanofibrils (CNF; or nanofibrillated cellulose,
94 NFC); and cellulose nanocrystals (CNCs). CNC elements are much shorter than both MFC and
95 CNF and does not have, therefore, the same ability as the MFC and CNF elements to form
96 networks. Various definitions may be found in the literature, but in the proposal for the new
97 TAPPI Standard, MFC have widths in the range of 10–100 nm, while CNF have widths of 5–30
98 nm (Wernersson Brodin, Gregersen & Syverud, 2014). Cellulose derivatives are among the most
99 employed natural fillers for the genaration of composite materials (Klemm et al., 2011; Faruk,
100 Bledzki, Fink & Sain, 2012). MFC, in particular, has successfully been used in the food packaging
101 field to produce composite films and coatings to improve barrier properties—for example, against
102 oxygen (Hult, Iotti & Lenes, 2010; Minelli et al., 2010) and water vapor (Azeredo et al., 2009;
103 Azeredo et al., 2010; Kaushik, Singh & Verma, 2010)—mechanical properties (Peng, Ren, Zhong
104 & Sun, 2011; Hansen, Blomfeldt, Hedenqvist & Plackett, 2012; Cozzolino, Cerri, Brundu &
105 Farris, 2014), thermal properties (Tingaut, Zimmermann & Lopez-Suevos, 2009; Joonobi, Harun,
106 Mathew & Oksman, 2010), and the antimicrobial attribute of the final package (Cozzolino et al.,

2013; Lavoine et al., 2014a,b,c; Lavoine, Desloges, Manship & Bras, 2015; Saini, Belgacem, Mendes, Elegir & Bras, 2015).

The objective of this study was to investigate the potential advantages eventually coming from the association of borax and MFC as fillers included in the main biopolymer matrix pullulan. In particular, the composite materials were developed in the form of thin coatings aiming to improve the oxygen and water barrier, mechanical, optical, and surface properties of a BOPP film, a commonly-used plastic for food packaging applications.

2. Experimental

2.1. Materials

Bi-oriented polypropylene (BOPP) 20.0 ± 0.5 μm thick was provided by Radici Film, S. Giorgio di Nogaro, Italy. Pullulan powder (PI-20 grade) was provided by Hayashibara Biochemical Laboratories, Inc. (Okayama, Japan). Structural characteristics of pullulan (determined by high-performance size exclusion chromatography equipped with multi-laser scattering and refractive index detectors – HPSEC-MALLS-RI) are: weight average molar mass (M_w) = 2.094×10^5 ± 0.002; polydispersity index (M_w/ M_n) = 1.321 ± 0.02; radius of gyration (R_g) = 24.7 ± 0.002 nm (Xiao, Tong, Zhou & Deng, 2015). Borax powder (sodium tetraborate decahydrate—$Na_2B_4O_7 \cdot 10H_2O$, purity > 99.5%, Mw= 381.37 g mol^{-1}) was purchased from Sigma-Aldrich. Milli-Q water (18.3 MΩ·cm) was used during the preparation of the pullulan-based films. All reagents were used as received.

MFC was produced at the Paper and Fibre Research Institute (PFI, Trondheim, Norway) by two different types of cellulose: (I) ECF (elemental chlorine free) fully bleached sulphate pulp mainly based on juvenile *Picea abies*, and (II) ECF (elemental chlorine free) fully bleached

sulphate cellulose mainly based on mature *Picea abies* with up to 5 wt.% pine (*Pinus sylvestris*), according to the same manufacturing procedure described by Turbak et al. (1983) and Herrik et al. (1983). The main physicochemical characteristics of the MFC used in this work are fully described in previous papers (Syverud & Stenius, 2009; Iotti, Gregersen, Moe & Lenes, 2011; Cozzolino, Cerri, Brundu & Farris, 2014).

2.2. Composites coatings preparation

Five different pullulan water solutions (2.0 wt.% wet basis) were prepared by mixing the pullulan powder in cold water under gentle stirring (500 rpm) for 1 h at room temperature. As displayed in Table 1, each solution was used as a batch to obtain five different formulations: 1) pristine pullulan solution, coded as P, which was used as a control; 2) P, also including borax (0.04 g/0.2 g pullulan, i.e. 0.4 wt.% wet basis), coded as P/B; 3) P, also including borax at a higher amount (0.1 g/0.2 g pullulan, i.e. 1 wt.% wet basis), coded as P/B+; 4) P/B, also including MFC (0.087 g/0.2 g pullulan, i.e. 0.87 wt.% wet basis), coded as P/B/MFC; 5) P/B+, also including MFC (0.87 wt.%), coded as P/B+/MFC. Borax and MFC were directly added to the main pullulan water solution and mixed by gentle stirring for 4 hrs in a climatic room (25 ± 0.5 °C). The obtained water solutions/dispersions were then left to rest for 24 hrs before usage.

To enhance the adhesion between coating and the plastic substrate, a two-step procedure was firstly adopted. In a first step, the BOPP was surface-activated using an Arcotec® "corona" generator model CG 061 P (Mönsheim, Germany). A chemical primer (0.5 wt% aziridine homopolymer water/ethanol solution) was deposited in a second step on the corona-treated BOPP to promote the adhesion between substrate and coating.

Table 1. Formulations of the different coatings prepared in this work.

Coating code	Pullulan		Borax		MFC		Solids	Water
	g	%	g	%	g	%	%	%
P	0.2	2	/	/	/	/	2	98
P/B	0.2	2	0.04	0.4	/	/	2.4	97.6
P/B+	0.2	2	0.1	1	/	/	3	97
P/B/MFC	0.2	2	0.04	0.4	0.087	0.87	3.27	96.73
P/B+/MFC	0.2	2	0.1	1	0.087	0.87	3.87	96.13

The deposition of the primer was performed by means of an automatic film applicator (Ref. 1137, Sheen Instruments, Kingston, UK) equipped with a steel horizontal rod with an engraved pattern, enabling the deposition of a layer having a nominal thickness of 0.02 μm. To promote the evaporation of the solvent, a constant and perpendicular flux of mild air (25.0 ± 0.3 °C for 2 min) at a distance of 40 cm from the applicator was used. Afterward, a first deposition of the coating solution/dispersion was done by means of an engraved rod enabling the deposition of a nominal wet thickness of 24.0 μm. After solvent removal, a second layer of the same water solution/dispersion was laid down. Coating deposition was performed according to ASTM D823-07, Practice C, at a constant speed of 150 mm min^{-1}.

All films were stored in a desiccator at 23 °C under dry conditions (using calcium chloride) for additional two weeks before analyses.

2.3 Analyses

2.3.1. Overall morphology and thickness determination

Field-emission scanning electron microscopy (FE-SEM) micrographs were obtained to acquire more detailed information on the morphology and global organization of the coating surface, e.g. to gather a qualitative evaluation of the increase in roughness of the pullulan coating after the addition of MFC. Cross-sectional images allowed to evaluate the adhesion behavior of the coating to the plastic substrate as well as to quantify the thickness of the final composite coatings. Both cross-sections and surfaces of the samples were examined using a Hitachi S-4800 FE-SEM (Schaumburg, IL, USA). Surface test specimens were mounted with carbon tape on stubs and cross-sectioned samples were cut into thin pieces with a scalpel and mounted in a 45 ° angle to the sample holders before insertion into the microscope. The samples were sputter-coated with platinum-palladium to a thickness of approximately 10 nm (to avoid charging the samples) using an Agar High Resolution Sputter Coater (model 208RH) equipped with a Pt/Pd target/Agar thickness monitor controller. Examination was carried out at 1 kV and a current of 10 μA.

The thickness of the biocomposite coatings was also evaluated using an optical microscope (Micro Nikon Eclipse ME600 Laboratory Imaging, Nikon Instruments, Sesto Fiorentino, Italy) at 100× magnification. Coated films after storage were fixed on a rectangular steel holder, and a sharp razor blade was used to perform cross-sectional observation. The thickness of the layers was obtained by a software-assisted procedure using the software NIS-Element (Nikon Instruments).

2.3.2. Infrared spectroscopy

Infrared spectra of the BOPP coated films were recorded using a PerkinElmer FT-IR Spectrum 100 Series spectrometer (PerkinElmer, Waltham, MA) equipped with a universal attenuated total

193 reflectance (UATR) accessory featuring a single-reflection sampling plate. To gather the spectral
194 information of the coatings, BOPP coated films were placed on the sampling plate with the
195 coating layer facing the 1.8 mm round germanium surface. The spectra were recorded over a
196 range of 650–4000 cm^{-1} with a resolution of 4 cm^{-1}, and averaged over 10 scans. Spectrum 6.0
197 software was used for data acquisition and analysis.
198
199 *2.3.3. Mechanical properties*
200 Mechanical tests were carried out using a Zwick Roell model Z005 dynamometer (Ulm,
201 Germany) and the software TestXpert V10.11 Master for data analysis. Elastic modulus (Emod,
202 MPa), elongation at break (ε, %) and tensile strength (TS, GPa) of films were measured according
203 to the ASTM D882-02 using a 5 kN load cell connected with two clamps placed at a distance of
204 125 mm from one another. The elastic modulus was drawn by a software-assisted procedure based
205 on a "secant" method; elongation at break was calculated dividing the extension-at-break of the
206 sample by the initial gauge length and multiplying by 100; TS was calculated using the equation
207 TS = F/A, where TS is the tensile strength in MPa, F is the force in N at maximum load, and A is
208 the initial cross-sectional area (mm^2) of the film sample.
209 Both static (μ_s) and kinetic (μ_k) coefficients of friction (COF) of films were determined in a
210 typical "coating vs. metal" configuration with the goal of simulating the friction between the
211 plastic web and the metallic parts of the equipment used during the manufacturing process. Tests
212 were carried out according to the ASTM D882-02, by means of a dynamometer (model Z005,
213 Zwick Roell, Ulm, Germany) fitted with a 100 N load cell. For each parameter, results are the
214 mean of at least ten replicates.
215

2.3.4. Optical properties

Haze was measured within the wavelength range 780−380 nm, in accordance with ASTM D 1003-00, using a UV-Vis high-performance spectrophotometer (Lambda 650, PerkinElmer, Waltham, MA, USA) coupled with a 150 mm integrating sphere, which allows trapping of the diffuse transmitted light. The final data are the average of three replicates.

2.3.5. Oxygen and water vapor barrier properties

The oxygen and water vapor barrier properties of both uncoated and coated PET films were assessed on a 50 cm^2 surface sample using a MultiPerm permeability analyzer (ExtraSolution® Srl, Capannori, Italy) equipped with an electrochemical sensor. Oxygen transmission rate (O_2TR, mL m^{-2} $24h^{-1}$) data were determined at 23 °C according to the standard method ASTM F2622-08, with a carrier flow (N_2) of 10 mL min^{-1} and one atmosphere pressure difference on the two sides of the specimen. Analyses were carried out with the coated side of each sample facing the upper semi-chamber where the humid test gas (oxygen) was fluxed. Two different relative humidity values were adopted, i.e., 0% and 70%.

The water vapor transmission rate (*WVTR*, g m^{-2} $24h^{-1}$) was measured according to the standard method ASTM F1249-05, with a carrier flow (N_2) of 10 mL min^{-1}, at 23 °C and 65% RH (temperate conditions) and 38°C and 90% RH (tropical conditions). For both O_2TR and *WVTR* analyses, final values resulted from three replicate measurements.

2.3.6. Contact angle analysis

Contact angle measurements were performed using an optical contact angle apparatus (OCA 15 Plus, Data Physics Instruments GmbH, Filderstadt, Germany) equipped with a high-resolution

CCD camera and a high performance digitizing adapter. SCA20 (Data Physics Instruments GmbH, Filderstadt, Germany) was used for contact angle measurements. Rectangular (5 × 2 cm^2) specimens were fixed and kept flat throughout the analysis by means of a special sample holder with parallel clamping jaws. The static contact angle of water in air (θ, °) was measured by the sessile drop method, by gently dropping a droplet of 4.0 ± 0.5 µL of Milli-Q water (18.3 MΩ cm) onto the substrate, according to the so-called pick-up procedure (a droplet hanging down from the needle is laid on a solid surface by raising the sample stage until solid/liquid contact is made) at 23 ± 1 °C and 50 ± 2% relative humidity (RH). The contact angle was recorded after 60 s from the droplet deposition, in order to allow the thermodynamic equilibrium between the three phases (solid, liquid, air) to be achieved (Farris et al., 2011). All droplets were released from a height of 1 cm above the surface to ensure consistency between each measurement. The static contact angle was measured as the angle between the baseline of the drop and the tangent at the drop boundary.

2.4. Statistical analysis

Statistical significance of differences between mean values was determined by one-way analysis of variance (ANOVA) using Statgraphic Plus 4.0 software. The mean values, where appropriate, were compared by Student's *t*-test with a significance level (p) < 0.05.

3. Results and discussion

3.1. Overall morphology and thickness of the composite coatings

FE-SEM images showed a very even and uniform deposition of the coating on the plastic substrate, namely neither empty (uncoated) areas nor discontinuities were observed for all the coating formulations (Figure 2a–c).

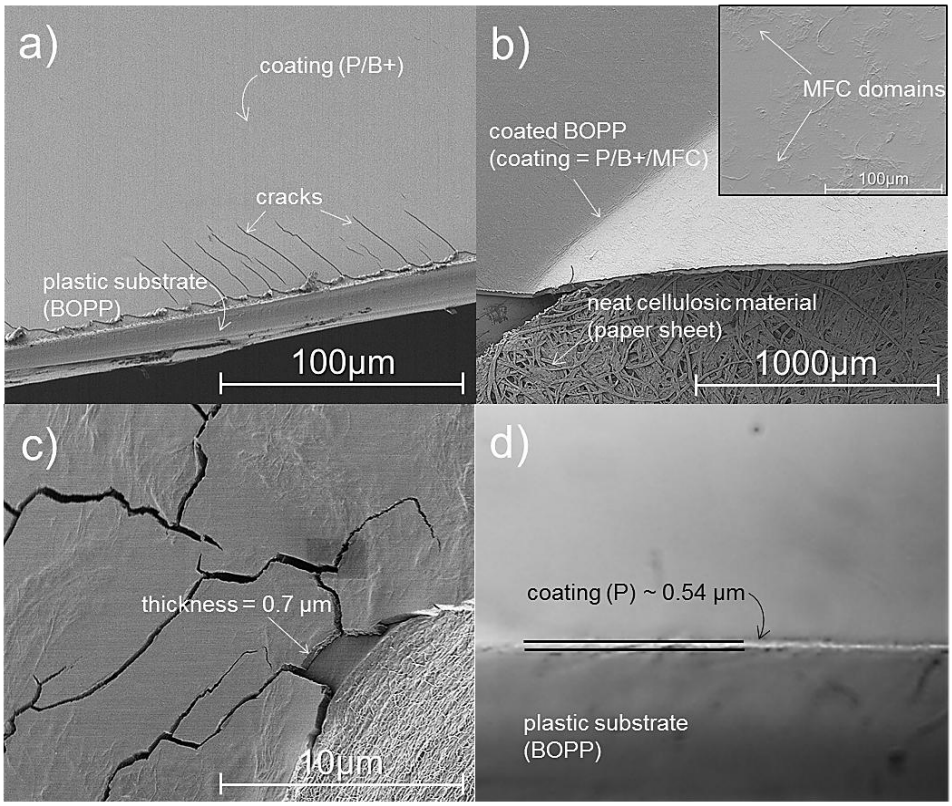

Figure 2. (a–c). FE-SEM micrographs of the BOPP plastic substrate coated with the composite formulations P/B+ (a) and P/B+/MFC (b and c). In panel (b), a bare cellulosic material has been taken as a reference to highlight the smoother surface of the MFC-loaded coating. In panel (c), the large fractures have been generated by the high energy level involved in the electrons touching the coating surface. (d) Optical microscopy image (cross-section) of the BOPP substrate coated with pullulan.

Some cracks occurred only in proximity of the fractured edges of the coated film, due to extensive mechanical stress (tearing) during sample preparation (Figure 2a). The addition of MFC did not dramatically change the overall morphology of the coating surface, with fiber dimension well below the typical size of bare cellulosic materials (Figure 2b). However, at higher magnifications

it was possible to detect an increase in surface roughness (Figure 2b, inset). The slight increase in surface roughness was spotty and associated with occasional presence of embedded MFC clusters (resulting in a maximum ca. 50 nm thickness increase), whereas the addition of borax did not change significantly the morphology of the coating surface, even at the highest concentration. Cross-sectional images showed that no delamination occurred at the BOPP/coating interface after coating deposition and solvent evaporation, unless excessive mechanical action was applied.

FE-SEM images (Figure 2c) and cross-sectional images obtained by the optical microscope (Figure 2d) allowed the determination of the thickness of the composite coatings (Table 2). The final thickness varied from 20.52 to 20.74 μm, which means that the coating thickness varied from 0.52 to 0.74 μm depending on the formulation. In addition, the optical microscopy images confirmed the adhesion between coating and BOPP even after cutting the sample by a razor. This support the important role of the primer in enhancing the adhesion strength at the coating/BOPP interface.

3.2. Infrared spectroscopy

The full-range FTIR/UATR spectra of pristine pullulan, MFC, and borax phases, together with the borax-richest composites P/B+ and P/B+/MFC, are shown in Figure S1 of Supporting Information, whereas the relevant peaks for the three phases (i.e., P, B, and MFC) are summarized in Table 3. Figure 3 displays two different spectral regions of interest. Within the range 3800–2700 cm^{-1} (panel a), the typical band of O–H stretching is evident for both pullulan (3352 cm^{-1}) and MFC (3342 cm^{-1}). It is likely that the different shape of this band (broad and large for pullulan, sharp for MFC) reflects structural differences between the two biopolymers—pullulan is a fully amorphous biopolymer, whereas MFC has been reported to have a crystallinity between

Table 2. Thickness (*l*), Young's modulus (Emod), elongation at break (ε), tensile strength (TS), and coefficient of friction (COF, static and dynamic) of bi-oriented polypropylene (BOPP) and BOPP coated with pullulan (P), pullan with borax (P/B), pullulan with high amount of borax (P/B+), pullulan with borax and MFC (P/B/MFC) and pullulan with high amount of borax and MFC (P/B+/MFC).

Sample	*l* (μm)	Emod (GPa)	TS (MPa)	ε (%)	COF μ_s	COF μ_k
BOPP	$20.00^{a} \pm 0.05$	$2.00^{a} \pm 0.40$	$98.53^{ab} \pm 32.08$	$58.18^{a} \pm 30.11$	$0.44^{a} \pm 0.03$	$0.33^{a} \pm 0.03$
P	$20.52^{a} \pm 0.04$	$2.01^{a} \pm 0.60$	$75.32^{a} \pm 31.68$	$38.65^{a} \pm 29.80$	$0.47^{ab} \pm 0.01$	$0.33^{a} \pm 0.01$
P/B	$20.49^{a} \pm 0.08$	$2.53^{ab} \pm 0.81$	$89.98^{ab} \pm 33.81$	$45.23^{a} \pm 26.56$	$0.50^{b} \pm 0.03$	$0.36^{b} \pm 0.02$
P/B+	$20.58^{a} \pm 0.06$	$2.79^{b} \pm 0.48$	$82.36^{ab} \pm 26.60$	$39.0^{a} \pm 22.32$	$0.45^{a} \pm 0.03$	$0.33^{a} \pm 0.01$
P/B/MFC	$20.68^{b} \pm 0.09$	$2.80^{b} \pm 0.81$	$113.62^{b} \pm 28.07$	$64.40^{a} \pm 23.46$	$0.34^{c} \pm 0.01$	$0.25^{c} \pm 0.01$
P/B+/MFC	$20.74^{b} \pm 0.06$	$3.08^{b} \pm 0.30$	$101.48^{ab} \pm 19.73$	$55.27^{a} \pm 17.56$	$0.35^{c} \pm 0.01$	$0.26^{c} \pm 0.01$

Results are expressed as mean values and standard deviation. Different superscripts within a group (i.e., within each parameter) denote a statistically significant difference ($p < 0.05$).

~ 50% and 80%, depending on several factors, such as the origin of the cellulosic material and the extraction method (Moon et al., 2011; Fei, Mascheroni & Piergiovanni, 2015). In addition, the MFC spectrum displays a less evident shoulder at 3285 cm^{-1} besides the main peak at 3342 cm^{-1}, which is probably due to the existence of different types of hydrogen bonds within the crystal lattice of MFC (Nishiyama et al., 2008). The peak at ~ 2928 cm^{-1} is attributed to the C–H stretching of the CH_2 group.

313 **Table 3.** Peak assignment for pullulan, microfibrillated cellulose and borax.

Pullulan		MFC		Borax	
Band (cm^{-1})	Assignment	Band (cm^{-1})	Assignment	Band (cm^{-1})	Assignment
848	$^4C_1$ chair conformation	1040–1060	C–O stretching	650	bending of B–O–B linkages within borate networks
929	α–(1→6)linkages	1110	C–O stretching	828	B–O stretching from residual $B(OH)_{4-}$
1021	C_4–O stretching	1162	C–O–C stretching	1410	asymmetric stretching relaxation of B–O–C (trigonal complexes)
1081	C_6–OH stretching	1315	C–H_2 wagging	1354	asymmetric stretching relaxation of B–O–C (tetrahedral complexes)
1154	C–O–C stretching	1372	C–H bending		
1354	C_6–OH bending	3340	O–H stretching		
1641	O–C–O stretching and glycosidic bridge				
2926.8	C–H stretching				
3346	O–H stretching vibration				

314 Adapted from Cozzolino *et al.*, 2015 and Spoljaric *et al.*, 2014.

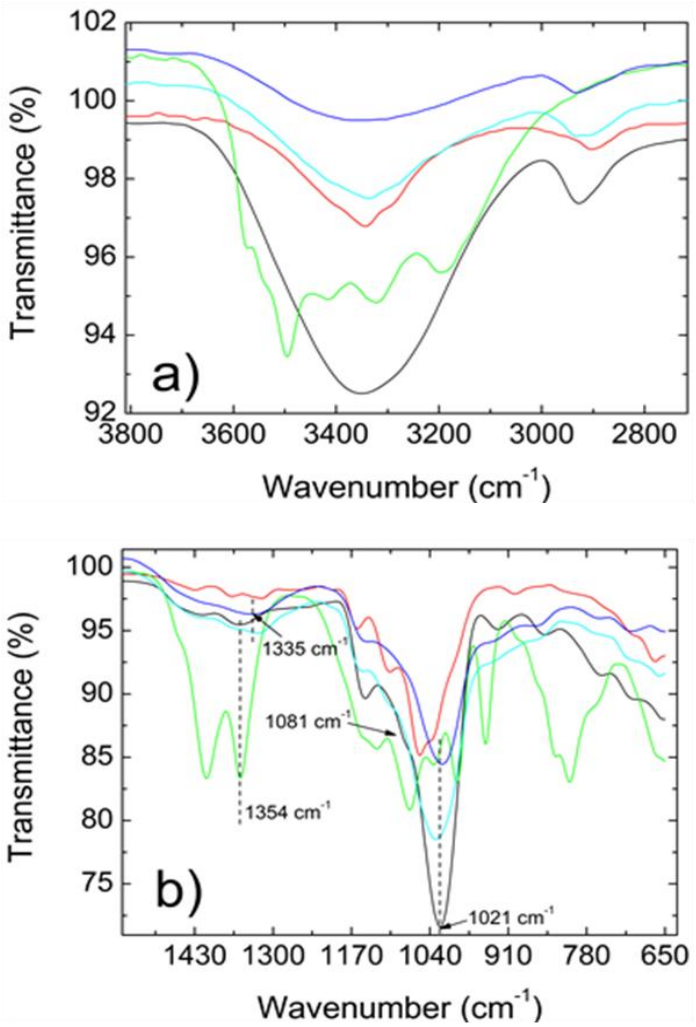

315

316 **Figure 2.** FTIR-UATR spectra of pullulan (P, black line), microfibrillated cellulose (MFC, red
317 line), borax (B, green line) and composite formulations P/B+ (blue line) and P/B+/MFC (cyan
318 line) within the spectral regions 3800–2700 cm^{-1} (a) and 1550–650 cm^{-1} (b). (Color figure
319 online).

320

321 No clear difference was observed between P and the composites P/B+ and P/B+/MFC in
322 correspondence of both O–H and C–H peaks in terms of shifting, broadening, etc., while the
323 different peak intensity is related to the relative amount of components used in the starting

formulation. The same observation was done for PVA/chitosan/borax films (Liang, Liu, Huang & Yam, 2009) and PVA/NFC/borax films (Spoljaric, Salminen, Dang Luong, & Seppälä, 2014). The authors concluded that hydrogen bonding was not the preferential way of interaction between the two biopolymers and borax.

Some spectral differences can be viewed within the spectral region 1550–650 cm^{-1} (panel b). If we consider the spectrum of pullulan (the main phase in all the composite coatings) as the reference spectrum for comparison purposes, it can be seen that the addition of the inorganic compound led to a clear shifting of the peak centered at 1354 cm^{-1} assigned to the C_6–OH bending (black line) to 1335 cm^{-1} (blue line). This suggests that the hydroxyl group on C_6 of the pullulan backbone was involved in the interaction with borax, probably via hydrogen bonding with the hydroxyl groups offered by boric acid. In addition, if we look at the shoulder positioned at ~ 1081 cm^{-1} of the pullulan spectrum (black line), which is assigned to the C_6–OH stretching, it completely disappeared in the P/B+ spectrum (blue line). This observation seems to disclose another kind of interaction, most likely the so-called monodiol and didiol complexation between vicinal diol units of pullulan chains and monoborate ions (Angelova et al., 2011), already postulated for other –OH-rich polymers, such as PVOH and cellulose (Han, Lei & Wu, 2014; Spoljaric, Salminen, Dang Luong & Seppälä, 2014).

We made another observation concerning the peak centered at 1021 cm^{-1} assigned to the C_4–O stretching in the pullulan spectrum (black line), which slightly shifted towards lower wavenumbers (blue line). It is plausible that this is due to conformational changes on the pullulan backbone in correspondence of the α–(1→4) linkage arising from the interaction between pullulan and borax. Keeping the peak at 1021 cm^{-1} as a reference, we noticed that it shifted towards higher wavenumbers in the composite coatings P/B+/MFC (cyan line), suggesting that conformational

changes occurred on the pullulan backbone because of the interaction with MFC, presumably governed by hydrogen bonding and van der Waals forces, possibly with the presence of water molecules (Han, Lei & Wu, 2014). No clear evidence of the main characteristic peaks of borax can be drawn from the spectral patterns obtained, mainly due to some overlapping bands, especially within the ~ 1500–1000 cm^{-1} range.

It can be concluded that the final conformation of the biocomposite coating network ensues from a balance between physical interactions (e.g., hydrogen bonding and van der Waals forces) and probably the formation of stable complexes according with the monodiol and didiol complexation schemes.

3.3. Mechanical properties

The results arising from the tensile test are summarized in Table 2. The deposition of pullulan did not influence the elastic modulus of the neat BOPP nor both tensile strength and elongation, which can be ascribed to the lack of crystallinity and high flexibility of the pullulan structure. The addition of borax led to an increase in the elastic modulus only at the highest concentration (from ~ 2 GPa of BOPP to ~ 2.79 GPa of the P/B+ coated BOPP films), i.e., when the formation of the "pullulan-borax" complexes (monodiol and didiol complexes) significantly affected the segmental mobility of the pullulan chains. No significant changes in terms of tensile strength and elongation were detected after the addition of borax. The highest elastic modulus of the biocomposite-coated films was recorded for the formulation P/B+/MFC (~ 3.08 GPa). This increase in stiffness—besides synergistic effects between MFC and borax— reflects the fibrillar nature of MFC, which has been widely used because of its reinforcing properties to obtain biocomposite materials with high specific strength and stiffness (Iwamoto, Yamamoto, Lee & Endo, 2014). Moreover, the significant increase in the elastic

modulus is clear evidence of the excellent interfacial adhesive interaction between the plastic substrate (BOPP) and the biocomposite coating, together with the ability of MFC fibrils to form a rigid network (Lavoine, Desloges, Dufresne & Bras, 2012), while preserving both tensile strength and plastic deformation of the original BOPP films.

As far as the friction properties are concerned, the most evident effect is due to the addition of MFC, which yielded a decrease of both static and kinetic coefficients of friction of approximately 22% and 25%, respectively, as compared to the neat BOPP. This effect is due to the increase in surface roughness due to the addition of MFC. As we demonstrated in our previous work, the inherent fibrillated nature of MFC yielded a crinkly surface morphology after deposition (Cozzolino, Cerri, Brundu & Farris, 2014), with final surface roughness (root-mean-square roughness, RMS) values in the order of 800 nm, which is much higher than that of bare BOPP (RMS ~ 10 nm) (Lin, Dias, Chum, Hiltner & Baer, 2007). The presence of a "peak-valley" morphology reduced the effective contact area between coating and metal, thus reducing the friction at the interface.

3.4. Optical properties

Quantification of haze, defined as the percentage of transmitted light deviating by more than an angle of 2.5° from the direction of the incident beam, is important, especially from a commercial point of view, as it is responsible for the reduction in the contrast between objects viewed through the specimen. In some cases (e.g., food packaging), when visual inspection through the material must be preserved, it is of the utmost importance to minimize the haze value of the materials to allow an adequate display of the product across the package (Cozzolino, Cerri, Brundu & Farris, 2014).

393 **Table 4.** Haze (%) and contact angle (θ, °) of bi-oriented polypropylene (BOPP) and BOPP
394 coated with pullulan (P), pullan with borax (P/B), pullulan with high amount of borax (P/B+),
395 pullulan with borax and MFC (P/B/MFC) and pullulan with high amount of borax and MFC
396 (P/B+/MFC).

Sample	Haze (%)	θ (°)
BOPP	$0.53^{a} \pm 0.03$	$78.49^{a} \pm 5.75$
P	$0.61^{a} \pm 0.08$	$23.08^{b} \pm 1.40$
P/B	$0.50^{a} \pm 0.02$	$21.27^{b} \pm 0.94$
P/B+	$0.55^{a} \pm 0.04$	$17.54^{c} \pm 1.46$
P/B/MFC	$10.02^{b} \pm 4.02$	$18.04^{c} \pm 1.77$
P/B+/MFC	$9.48^{b} \pm 0.52$	$17.73^{c} \pm 1.27$

397 Results are expressed as mean values and standard deviation. Different superscripts within a
398 group (i.e., within each parameter) denote a statistically significant difference ($p < 0.05$).

399

400 The experimental haze values (%) are reported in Table 4. The deposition of pullulan and
401 pullulan-borax coatings did not significantly affect the original optical property of the neat BOPP.
402 This indicates an even dispersion of the inorganic phase into the pullulan main matrix, with no
403 formation of scattering centers. Conversely, the addition of MFC to the pullulan-borax
404 formulation caused a dramatic increase in haze, from ~ 0.55 % to ~ 10%. Also in this case, the
405 higher surface roughness of the MFC-based coatings is the reason for this behavior, because the
406 wrinkled/jagged surface morphology enhances the diffusion of the incident light (Tilley, 2011).
407 However, the formation of MFC aggregates on the films surface might have contributed to the
408 increase in haze values.

Table 5. *O_2TR* and *WVTR* values of bi-oriented polypropylene (BOPP) and BOPP coated with pullulan (P), pullan with borax (P/B), pullulan with high amount of borax (P/B+), pullulan with borax and MFC (P/B/MFC) and pullulan with high amount of borax and MFC (P/B+/MFC).

Sample	*O_2TR* (mL m^{-2} $24h^{-1}$)		*WVTR* (g m^{-2} $24h^{-1}$)	
	23 °C 0% RH	23 °C 80% RH	23 °C 65% RH	38 °C 90% RH
BOPP	$866.61^{a} \pm 2.18$	$886.77^{a} \pm 1.50$	$1.13^{a} \pm 0.06$	$6.73^{a} \pm 0.03$
P	$4.96^{b} \pm 0.05$	$319.88^{b} \pm 0.74$	$1.13^{a} \pm 0.06$	$6.60^{b} \pm 0.02$
P/B	$1.03^{c} \pm 0.06$	$290.30^{c} \pm 1.08$	$1.11^{a} \pm 0.09$	$6.61^{b} \pm 0.11$
P/B+	$5.43^{b} \pm 0.07$	$316.82^{d} \pm 0.34$	$1.17^{a} \pm 0.04$	$6.94^{c} \pm 0.09$
P/B/MFC	$2.97^{d} \pm 0.06$	$191.46^{e} \pm 0.47$	$1.16^{a} \pm 0.05$	$6.63^{ab} \pm 0.04$
P/B+/MFC	$5.17^{b} \pm 0.07$	$206.70^{f} \pm 0.30$	$1.14^{a} \pm 0.05$	$6.61^{b} \pm 0.02$

Results are expressed as mean values and standard deviation. Different superscripts within a group (i.e., within each parameter) denote a statistically significant difference ($p < 0.05$).

3.5. Oxygen and water vapor barrier properties

The barrier properties against oxygen and water vapor of neat BOPP, pullulan-coated BOPP and BOPP coated with the biocomposite films are reported in Table 5. The deposition of the coatings dramatically decreased the original *O_2TR* value of the neat BOPP under dry conditions, which can be explained by the tight network formed by the pullulan and pullulan-based layers due to the extensive hydrogen bonding. The best performance was observed for the P/B formulation, whereas the highest amount of borax (P/B+ formulation) did not bring any benefit compared to the pullulan-coated BOPP films. It is likely that borax at low concentration acted as a true filler, reducing the free volume of the main biopolymer phase via hydrogen bonding. At a higher concentration, it is plausible that borax exceeded the inherent intermolecular porosity of the

pullulan network. As observed for other composite systems, this could have originated an aggregation phenomena and formation of macro-domains segregated from the main polymer phase, which causes depletion in the barrier performance following an increase in the free volume of the polymer matrix (Wilson et al., 2011). In the formulation P/B/MFC, the addition of the cellulosic material decreased significantly the O_2 barrier performance of the P/B composite, whereas it did not affected the O_2TR value of the P/B+ formulation. In principle, the addition of MFC would seem to increase the oxygen barrier performance due to both newly formed hydrogen bonds and high crystallinity. However, other parameters, such as physical entanglement and nanoporosity of the web-like MFC network, may considerably affect the final barrier performance of the composite (Lavoine, Desloges, Dufresne & Bras, 2012).

At 80% RH, the O_2TR values of BOPP-coated films increased dramatically, though still well below the O_2TR value of the neat BOPP films. Such a decrease in the O_2TR values at high RHs can be attributed to the sensitivity of the biocomposite coatings to water moisture. At 80% RH, water molecules limit the hydrogen bonds, creating films that are less packed (Aulin, Gällstedt & Lindström, 2010) due to swelling of the hydrophilic network (Wernersson Brodin, Gregersen & Syverud, 2014).

As far as the *WVTR* results are concerned, it can be clearly seen that the addition of the coatings on the BOPP substrate did not bring any sort of advantage, regardless of the formulation used and irrespective of the conditions of analysis adopted (temperate or tropical). The high affinity towards water molecules remains the main reason for the observed behavior, especially at high temperatures.

448 3.6. Contact angle analysis

449 Water contact angle data are displayed in Table 4. The deposition of the pullulan coating
450 decreased the high water contact angle of neat BOPP ($\theta \sim 80°$), which is well known for its non-
451 wetting behavior due low surface energy values of ~ 28 mJ m^{-2} (Farris et al., 2014b). Pullulan
452 coatings showed the lowest water contact angle among several biopolymer coatings (~ 23° after
453 60 s upon droplet deposition) (Farris et al., 2011). This behavior accounts for some
454 physicochemical features of this exopolysaccharide, in particular, high hydroxyl groups content
455 along the molecular skeleton (nine –OH groups per repeating unit–maltotriose) and a lack of
456 crystal domains, which concurrently made the interaction between the biopolymer and the water
457 molecules more favorable (Farris et al., 2014a).

458 The addition of borax at a low concentration did not significantly change the wettability of
459 the pullulan-coated BOPP surface. In line with previous comments, it is plausible that borax (e.g.,
460 boric acid) first filled the intermolecular voids of the main pullulan network interacting by
461 hydrogen bonds. Therefore, the hydroxyl groups of the filler cannot freely interact with the water
462 molecules on the coating surface. Instead, the addition of borax at a high amount as well as of
463 MFC had a significant impact on the wettability of the composite coatings. Excess of free
464 hydroxyl and polar groups at the solid/air interface increased the affinity towards water molecules,
465 thus the ability of water to wet the coating surface. In particular, it was observed that the highest
466 amount of borax and the addition of MFC yielded an increase in the spreading component of the
467 overall water contact angle at the equilibrium (i.e., after 60 s).

468

469

470

4. Conclusions

The addition of MFC and borax has successfully improved both mechanical and surface properties of pullulan coatings laid on the plastic substrate BOPP. In particular, the stiffness of the coated films was significantly improved without impairing the elongation at break. Moreover, the friction properties were not affected and yet improved upon the addition of MFC, which can be profitably exploited to speed up the manufacturing operation in the industrial plants. While borax did not affect the haze of the coated films, the use of MFC worsened the ability to see through the coated films due to the fibrillar nature of the cellulosic component and also slightly increased the coating surface roughness. The deposition of the biocomposite coatings allowed to achieve outstanding oxygen barrier performance, especially under dry conditions, compared to the poor performance of the plastic substrate. This configuration may find application in oxygen-sensitive dry foods (e.g., fat-containing biscuits), refrigerated products (e.g., ham), and possibly MAP-packaged vegetables requiring a moderate oxygen barrier performance to allow gas exchanges between the interior of the package and the external environment. Finally, composite coatings dramatically improved the wettability of the plastic substrate, allowing to switch from a hydrophobic "water-repellent" surface to a hydrophilic "wettable" surface. This may have a great impact on food packaging applications requiring anti-fog attributes, e.g., BOPP films for minimally processed fruits and vegetables.

References

Angelova, L. V., Terech, P., Natali, I., Dei, L., Carretti, E., & Weiss, R. G. (2011). Cosolvent gel-like materials from partially hydrolyzed poly(vinyl acetate)s and borax. *Langmuir, 27(18)*, 11671–11682.

Aulin, C., Gällstedt, M., & Lindström, T. (2010). Oxygen and oil barrier properties of microfibrillated cellulose films and coatings. *Cellulose, 17(3)*, 559–574.

Azeredo, H. M., Mattoso, L. H., Wood, D., Williams, T. G., Avena-Bustillos, R. J., & McHugh, T. H. (2009). Nanocomposite edible films from mango puree reinforced with cellulose nanofibers. *Journal of Food Science, 74*, 31–35.

Azeredo, H. M., Mattoso, L. H., Avena-Bustillos, R. J., Filho, G. C., Munford, M. L., Wood, D., & McHugh, T. H. (2010). Nanocellulose reinforced chitosan composite films as affected by nanofiller loading and plasticizer content. *Journal of Food Science, 75*, 1–7.

Barlow, C. Y., & Morgan, D. C. (2013). Polymer film packaging for food: an environmental assessment. *Resources, Conservation and Recycling 78*, 74–80.

Berglund, L. (2006). New concepts in natural fibres composites. 27th Risø international symposium on material science. Risø National Laboratory, Roskilde, Denmark.

Cabiaca, A., Guillon, E., Chambon, F., Pinel, C., Rataboul, F., & Essayem, N. (2011). Cellulose reactivity and glycosidic bond cleavage in aqueous phase by catalytic and non catalytic transformations. *Applied Catalysis A-General, 402*, 1–10.

513 Chinga-Carrasco, G., Miettinen, A., Luengo Hendriks, C. L., Gamstedt, E. K., & Kataja, M.
514 (2011). Structural Characterisation of Kraft Pulp Fibres and Their Nanofibrillated
515 Materials for Biodegradable Composite Applications. In: Nanocomposites and Polymers
516 with Analytical Methods - Book 3, ISBN 979-953-307-136-6 (pp. 243–260).

517 Cozzolino, C. A., Nilsson, F., Iotti, M., Sacchi, B., Piga, A., & Farris, S. (2013). Exploiting the
518 nano-sized features of microfibrillated cellulose (MFC) for the development of controlled
519 release packaging. *Colloids and Surfaces B-Biointerfaces*, *110*, 208–216.

520 Cozzolino, C. A., Cerri, G., Brundu, A., & Farris, S. (2014). Microfibrillated cellulose (MFC)−
521 pullulan bionanocomposite films. *Cellulose*, *21(6)*, 4323–4335.

522 EFSA ANS – Food additives & nutrient sources added to food, ANS Panel (2013). Scientific
523 Opinion on the re-evaluation of boric acid (E 284) and sodium tetraborate (borax) (E 285)
524 as food additives. EFSA Journal, 11(10), 3407 (52 pp.) doi:10.2903/j.efsa.2013.3407

525 Farris, S., Introzzi, L., & Piergiovanni, L. (2009). Evaluation of a Bio-coating as a Solution to
526 Improve Barrier, Friction and Optical Properties of Plastic Films. *Packaging Technology*
527 *And Science*, *22*, 69–83.

528 Farris, S., Introzzi, L., Biagioni, P., Holz, T., Schiraldi, A., & Piergiovanni, L. (2011). Wetting of
529 biopolymer coatings: contact angle kinetics and image analysis investigation. *Langmuir*,
530 *27(12)*, 7563–7574.

Farris, S., Introzzi, L., Fuentes-Alventosa, J. M., Santo, N., Rocca, R., & Piergiovanni, L. (2012). Self-assembled pullulan-silica oxygen barrier hybrid coatings for food packaging applications. *Journal of Agricultural and Food Chemistry, 60(3),* 782−790.

Farris, S., Uysal Unalan, I., Introzzi, L., Fuentes-Alventosa, J. M., & Cozzolino, C. A. (2014a). Pullulan-Based Films and Coatings for Food Packaging: Present Applications, Emerging Opportunities, and Future Challenges. *Journal of Applied Polymer Science, 131(13),* DOI: 10.1002/APP.40539.

Farris, S., Pozzoli, S., La Vecchia, S., Biagioni, P., Bianchi, C. L., & Piergiovanni, L. (2014b). Mapping physicochemical surface modifications of flame-treated polypropylene. *eXPRESS Polymer Letters, 8(4),* 256–266.

Faruk, O., Bledzki, A. K., Fink, H. P., & Sain, M. (2012). Biocomposites reinforced with natural fibers: 2000–2010. *Progress in Polymer Science, 37,* 1552–1596.

Fei, L., Mascheroni, E., & Piergiovanni, L. (2015). The potential of nanocellulose in the packaging field: A review. *Packaging Technology and Science, 28,* 475–508.

Han, J., Lei, T., & Wu, Q. (2014). High-water-content mouldable polyvinyl alcohol-borax hydrogelsreinforced by well-dispersed cellulose nanoparticles: Dynamicrheological properties and hydrogel formation mechanism. *Carbohydrate Polymers, 102,* 306–316.

Hansen, N. M. L., Blomfeldt, T. O. J., Hedenqvist, M. S., & Plackett, D. V. (2012). Properties of plasticized composite films prepared from nanofibrillated cellulose and birch wood xylan. *Cellulose, 19,* 2015–2031.

551 Herrick, F. W., Casebier, R. L., Hamilton, J. K., & Sandberg, K. R. (1983). Microfibrillated
552 Cellulose: Morphology and accessibility. *Journal of Applied Polymer Science: Appl.*
553 *Polym. Symp., 37,* 797–813.

554 Huang, Y., Zhu, C., Yang, J., Nie, Y., Chen, C., & Sun, D. (2014). Recent advances in bacterial
555 cellulose. *Cellulose, 21,* 1–30.

556 Hult, E. L., Iotti, M., & Lenes, M. (2010). Efficient approach to high barrier packaging using
557 microfibrillar cellulose and shellac. *Cellulose, 17,* 575–586.

558 Introzzi, L., Fuentes-Alventosa, J. M., Cozzolino, C. A., Trabattoni, S., Tavazzi, S., Bianchi, C.
559 L., Schiraldi, A., Piergiovanni, L., & Farris, S. (2012a). 'Wetting enhancer' pullulan
560 coating for anti-fog packaging applications. *ACS Applied Materials & Interfaces, 4,*
561 3692−3700.

562 Introzzi, L., Blomfeldt, T. O. J., Trabattoni, S., Tavazzi, S., Santo, N., Schiraldi, A., Piergiovanni,
563 L., & Farris, S. (2012b). Ultrasound-assisted pullulan/montmorillonite bionanocomposite
564 coating with high oxygen barrier properties. *Langmuir, 28,* 11206−1121.

565 Iotti, M., Gregersen, Ø. W., Moe, S., & Lenes, M. (2011). Rheological Studies of Microfibrillar
566 Cellulose Water Dispersions. *Journal of Polymers and the Environment, 19,* 137–145.

567 Iwamoto, S., Yamamoto, S., Lee, S. H., & Endo, T. (2014). Mechanical properties of
568 polypropylene composites reinforced by surface-coated microfibrillated cellulose.
569 *Composites: Part A, 59,* 26–29.

570 Jonoobi, M., Harun, J., Mathew, A. P., & Oksman, K. (2010). Mechanical properties of cellulose
571 nanofiber (CNF) reinforced polylactic acid (PLA) prepared by twin screw extrusion.
572 *Composites Science and Technology, 70,* 1742−1747.

573 Kaushik, A., Singh, M., & Verma, G. (2010). Green nanocomposites based on thermoplastic
574 starch and steam exploded cellulose nanofibrils from wheat straw, *Carbohydrate*
575 *Polymers, 82,* 337–345.

576 Klemm, D., Kramer, F., Moritz, S., Lindström, T., Ankerfors, M., Gray, D., & Dorris, A. (2011).
577 Nanocelluloses: A New Family of Nature-Based Materials. *Angewandte Chemie-*
578 *International Edition, 50,* 5438–5466.

579 Kristo, E., & Biliaderis, C. G. (2007). Physical properties of starch nanocrystal-reinforced
580 pullulan films. *Carbohydrate Polymers, 68,* 146–158.

581 Lavoine, N., Desloges, I., Dufresne, A. & Bras, J. (2012). Microfibrillated cellulose - Its barrier
582 properties and applications in cellulosic materials: A review. *Carbohydrate Polymers,*
583 *90(2),* 735–764.

584 Lavoine, N., Tabary, N., Desloges, I., Martel, B., & Bras, J. (2014a). Controlled release of
585 chlorhexidine digluconate using β-cyclodextrin and microfibrillated cellulose. *Colloids*
586 *and Surfaces B: Biointerfaces 121,* 196–205.

587 Lavoine, N., Desloges, I., Sillard, C., & Bras, J. (2014b). Controlled release and long-term
588 antibacterial activity of chlorhexidine digluconate through the nanoporous network of
589 microfibrillated cellulose. *Cellulose, 21,* 4429–4442.

590 Lavoine, N., Desloges, I., & Bras, J. (2014c). Microfibrillated cellulose coatings as new release
591 systems for active packaging. *Carbohydrate Polymers*, *103*, 528–537.

592 Lavoine, N., Desloges, I., Manship, B., & Bras, J. (2015). Antibacterial paperboard packaging
593 using microfibrillated cellulose. *Journal of Food Science and Technology*, *52*, 5590–5600.

594 Leathers, T. D. (2003). Biotechnological production and applications of pullulan. *Applied*
595 *Microbiology And Biotechnology*, *62*, 468–473.

596 Liang, S., Liu, L., Huang, Q., & Yam, K. L. (2009). Preparation of single or double-network
597 chitosan/poly (vinyl alcohol) gel films through selectively cross-linking method.
598 *Carbohydrate Polymers*, *77(4)*, 718–24.

599 Lin, Y. J., Dias, P., Chum, S., Hiltner, A., & Baer, E. (2007). Surface roughness and light
600 transmission of biaxially oriented polypropylene films. *Polymer Engineering and Science*,
601 *47(10)*, 1658–1665.

602 Minelli, M., Baschetti, M. G., Doghieri, F., Ankerfors, M., Lindström, T., Siró, I., & Plackett, D.
603 (2010). Investigation of mass transport properties of microfibrillated cellulose (MFC)
604 films. *Journal of Membrane Science*, *358*, 67–75.

605 Moon, R. J., Martini, A., Nairn, J., Simonsen, J., & Youngblood, J. (2011). Cellulose
606 nanomaterials review: structure, properties and nanocomposites. *Chemical Society*
607 *Reviews*, *40*, 3941–3994.

608 Nishiyama, Y., Johnson, G. P., French, A. D., Forsyth, V. T., & Langan, P. (2008). 'Neutron
609 crystallography, molecular dynamics, and quantum mechanics studies of the nature of
610 hydrogen bonding in cellulose I-β'. *Biomacromolecules, 9,* 3133–3140.

611 Peng, X. W., Ren, J. L., Zhong, L. X., & Sun, R. C. (2011). Nanocomposite films based on xylan-
612 rich hemicelluloses and cellulose nanofibers with enhanced mechanical properties.
613 *Biomacromolecules, 12,* 3321–3329.

614 Rhim, J. W., Park, H. M., & Ha, C. S. (2013). Bio-nanocomposites for food packaging
615 applications. *Progress in Polymer Science, 38,* 1629–1652.

616 Saini, S., Belgacem, N., Mendes, J., Elegir, G., & Bras, J. (2015). Contact antimicrobial surface
617 obtained by chemical grafting of microfibrillated cellulose in aqueous solution limiting
618 antibiotic release. *Applied Materials & Interfaces, 7,* 18076−18085.

619 Spoljaric, S., Salminen, A., Dang Luong, N., & Seppälä, J. (2014). Stable, self-healing hydrogels
620 from nanofibrillated cellulose, poly(vinyl alcohol) and borax via reversible crosslinking.
621 *European Polymer Journal, 56,* 105–117.

622 Syverud, K., & Stenius, P. (2009). Strength and barrier properties of MFC films. *Cellulose, 16,*
623 75–85.

624 Tilley, R. J. D. (2011). Colour and The Optical Properties of Materials, 2 edition. Wiley,
625 Hoboken, p. 42.

626 Tingaut, P., Zimmermann, T., & Lopez-Suevos, F. (2009). Synthesis and Characterization of
627 Bionanocomposites with Tunable Properties from Poly(lactic acid) and Acetylated
628 Microfibrillated Cellulose. *Biomacromolecules, 11*, 454−464.

629 Trovatti, E., Fernandes, S. C. M., Rubatat, L., da Silva Perez, D., Freire, C. S. R., Silvestre, A. J.
630 D., & Neto, C. P. (2012). Pullulan–nanofibrillated cellulose composite films with
631 improved thermal and mechanical properties. *Composites Science and Technology, 72*,
632 1556–1561.

633 Turbak, A. F., Snyder, F. W., & Sandberg, K. R. (1983). Microfibrillated cellulose, a new
634 cellulose product: properties, uses, and commercial potential. *Journal of Applied Polymer*
635 *Science: Appl. Polym. Symp. 37,* 815–827.

636 Unalan, I. U., Wan, C., Figiel, L. F., Olsson, R. T., Trabattoni, S., & Farris, S. (2015). Exceptional
637 oxygen barrier performance of pullulan nanocomposites with ultra-low loading of
638 graphene oxide. *Nanotechnology, 26 (27),* 275703.

639 Wernersson Brodin, F., Gregersen, Ø. W., & Syverud, K. (2014). Cellulose nanofibrils:
640 Challenges and possibilities as a paper additive or coating material – A review. *Nordic*
641 *Pulp & Paper Research Journal, 29(1),* 156–166.

642 Wilson, R., Plivelic, T. S., Aprem, A. S., Ranganathaiagh, C., Kumar S. A., & Thomas, S. (2011).
643 Preparation and Characterization of EVA/Clay Nanocomposites with Improved Barrier
644 Performance. *Journal of Applied Polymer Science, 123*, 3806–3818.

Wu, J., Zhong, F., Li, Y., Shoemaker, C. F., & Xia, W. (2013). Preparation and characterization of pullulan-chitosan and pullulan-carboxymethyl chitosan blended films. *Food Hydrocolloids, 30,* 82–91.

Xiao, Q., Lim, L. T., & Tong, Q. (2012). Properties of pullulan-based blend films as affected by alginate content and relative humidity. *Carbohydrate Polymers, 87,* 227–234.

Xiao, Q., Tong, Q., Zhou, Y., & Deng, F. (2015). Rheological properties of pullulan-sodium alginate based solutions during film formation. *Carbohydrate Polymers, 130,* 49–56.

Yanjuan, W., Yanxiong, F., Wei, T., & Chunying, L. (2013). Preservation of aged paper using borax in alcohols and the supercritical carbon dioxide system. *Journal of Cultural Heritage, 14,* 16–22.

Yuen, S. (1974). Pullulan and its applications. *Process Biochemistry, 9,* 7−9.

Yunus Gumus, O., Unal, H. I., Erol, O., & Sari, B. (2011). Synthesis, characterization, and colloidal properties of polythiophene/borax conducting composite. *Polymer Composites, 32(3),* 418–426.

663 Figure captions

664 **Figure 1.** a) pullulan molecule as a sequence of repeating units of maltotriose (adapted from
665 Farris et al., 2014); b) sodium tetraborate decahydrate; c) structure of cellulose (four molecular
666 chains to form a strand) with intra- and inter-molecular hydrogen bonds (dashed lines) in
667 evidence.

668 **Figure 2. (a–c).** FE-SEM micrographs of the BOPP plastic substrate coated with the
669 composite formulations P/B+ (a) and P/B+/MFC (b and c). In panel (b), a bare cellulosic
670 material has been taken as a reference to highlight the smoother surface of the MFC-loaded
671 coating. In panel (c), the large fractures have been generated by the high energy level involved
672 in the electrons touching the coating surface. (d) Optical microscopy image (cross-section) of
673 the BOPP substrate coated with pullulan.

674 **Figure 3.** FTIR-UATR spectra of pullulan (P, black line), microfibrillated cellulose (MFC, red
675 line), borax (B, green line) and nanocomposite formulations P/B+ (blue line) and P/B+/MFC
676 (cyan line) within the spectral regions 3800–2700 cm^{-1} (a) and 1550–650 cm^{-1} (b). (Color
677 figure online).

Table 1. Formulations of the different coatings prepared in this work.

Coating code	Pullulan		Borax		MFC		Solids	Water
	g	%	g	%	g	%	%	%
P	0.2	2	/	/	/	/	2	98
P/B	0.2	2	0.04	0.4	/	/	2.4	97.6
P/B+	0.2	2	0.1	1	/	/	3	97
P/B/MFC	0.2	2	0.04	0.4	0.087	0.87	3.27	96.73
P/B+/MFC	0.2	2	0.1	1	0.087	0.87	3.87	96.13

Table 2

Table 2. Thickness (*l*), Young's modulus (Emod), elongation at break (ε), tensile strength (TS), and coefficient of friction (COF, static and dynamic) of bi-oriented polypropylene (BOPP) and BOPP coated with pullulan (P), pullan with borax (P/B), pullulan with high amount of borax (P/B+), pullulan with borax and MFC (P/B/MFC) and pullulan with high amount of borax and MFC (P/B+/MFC).

Sample	*l* (μm)	Emod (GPa)	TS (MPa)	ε (%)	COF	
					μ_s	μ_k
BOPP	$20.00^{a} \pm 0.05$	$2.00^{a} \pm 0.40$	$98.53^{ab} \pm 32.08$	$58.18^{a} \pm 30.11$	$0.44^{a} \pm 0.03$	$0.33^{a} \pm 0.03$
P	$20.52^{a} \pm 0.04$	$2.01^{a} \pm 0.60$	$75.32^{a} \pm 31.68$	$38.65^{a} \pm 29.80$	$0.47^{ab} \pm 0.01$	$0.33^{a} \pm 0.01$
P/B	$20.49^{a} \pm 0.08$	$2.53^{ab} \pm 0.81$	$89.98^{ab} \pm 33.81$	$45.23^{a} \pm 26.56$	$0.50^{b} \pm 0.03$	$0.36^{b} \pm 0.02$
P/B+	$20.58^{a} \pm 0.06$	$2.79^{b} \pm 0.48$	$82.36^{ab} \pm 26.60$	$39.0^{a} \pm 22.32$	$0.45^{a} \pm 0.03$	$0.33^{a} \pm 0.01$
P/B/MFC	$20.68^{b} \pm 0.09$	$2.80^{b} \pm 0.81$	$113.62^{b} \pm 28.07$	$64.40^{a} \pm 23.46$	$0.34^{c} \pm 0.01$	$0.25^{c} \pm 0.01$
P/B+/MFC	$20.74^{b} \pm 0.06$	$3.08^{b} \pm 0.30$	$101.48^{ab} \pm 19.73$	$55.27^{a} \pm 17.56$	$0.35^{c} \pm 0.01$	$0.26^{c} \pm 0.01$

Results are expressed as mean values and standard deviation. Different superscripts within a group (i.e., within each parameter) denote a statistically significant difference ($p < 0.05$).

Table 3. Peak assignment for pullulan, microfibrillated cellulose and borax.

Pullulan		MFC		Borax	
Band (cm^{-1})	Assignment	Band (cm^{-1})	Assignment	Band (cm^{-1})	Assignment
848	$^4C_1$ chair conformation	1040–1060	C–O stretching	650	bending of B–O–B linkages within borate networks
929	α–(1→6)linkages	1110	C–O stretching	828	B–O stretching from residual $B(OH)_{4-}$
1021	C_4–O stretching	1162	C–O–C stretching	1410	asymmetric stretching relaxation of B–O–C (trigonal complexes)
1081	C_6–OH stretching	1315	C–H_2 wagging	1354	asymmetric stretching relaxation of B–O–C (tetrahedral complexes)
1154	C–O–C stretching	1372	C–H bending		
1354	C_6–OH bending	3340	O–H stretching		
1641	O–C–O stretching and glycosidic bridge				
2926.8	C–H stretching				
3346	O–H stretching vibration				

Adapted from Cozzolino *et al.*, 2015 and Spoljaric *et al.*, 2014.

Table 4

Table 4. Haze (%) and contact angle (θ, °) of bi-oriented polypropylene (BOPP) and BOPP coated with pullulan (P), pullan with borax (P/B), pullulan with high amount of borax (P/B+), pullulan with borax and MFC (P/B/MFC) and pullulan with high amount of borax and MFC (P/B+/MFC).

Sample	Haze (%)	θ (°)
BOPP	$0.53^{a} \pm 0.03$	$78.49^{a} \pm 5.75$
P	$0.61^{a} \pm 0.08$	$23.08^{b} \pm 1.40$
P/B	$0.50^{a} \pm 0.02$	$21.27^{b} \pm 0.94$
P/B+	$0.55^{a} \pm 0.04$	$17.54^{c} \pm 1.46$
P/B/MFC	$10.02^{b} \pm 4.02$	$18.04^{c} \pm 1.77$
P/B+/MFC	$9.48^{b} \pm 0.52$	$17.73^{c} \pm 1.27$

Results are expressed as mean values and standard deviation. Different superscripts within a group (i.e., within each parameter) denote a statistically significant difference ($p < 0.05$).

Table 5. *O_2TR* and *WVTR* values of bi-oriented polypropylene (BOPP) and BOPP coated with pullulan (P), pullan with borax (P/B), pullulan with high amount of borax (P/B+), pullulan with borax and MFC (P/B/MFC) and pullulan with high amount of borax and MFC (P/B+/MFC).

Sample	*O_2TR* (mL m^{-2} $24h^{-1}$)		*WVTR* (g m^{-2} $24h^{-1}$)	
	23 °C 0% RH	23 °C 80% RH	23 °C 65% RH	38 °C 90% RH
BOPP	$866.61^{a} \pm 2.18$	$886.77^{a} \pm 1.50$	$1.13^{a} \pm 0.06$	$6.73^{a} \pm 0.03$
P	$4.96^{b} \pm 0.05$	$319.88^{b} \pm 0.74$	$1.13^{a} \pm 0.06$	$6.60^{b} \pm 0.02$
P/B	$1.03^{c} \pm 0.06$	$290.30^{c} \pm 1.08$	$1.11^{a} \pm 0.09$	$6.61^{b} \pm 0.11$
P/B+	$5.43^{b} \pm 0.07$	$316.82^{d} \pm 0.34$	$1.17^{a} \pm 0.04$	$6.94^{c} \pm 0.09$
P/B/MFC	$2.97^{d} \pm 0.06$	$191.46^{e} \pm 0.47$	$1.16^{a} \pm 0.05$	$6.63^{ab} \pm 0.04$
P/B+/MFC	$5.17^{b} \pm 0.07$	$206.70^{f} \pm 0.30$	$1.14^{a} \pm 0.05$	$6.61^{b} \pm 0.02$

Results are expressed as mean values and standard deviation. Different superscripts within a group (i.e., within each parameter) denote a statistically significant difference ($p < 0.05$).

Figure 1

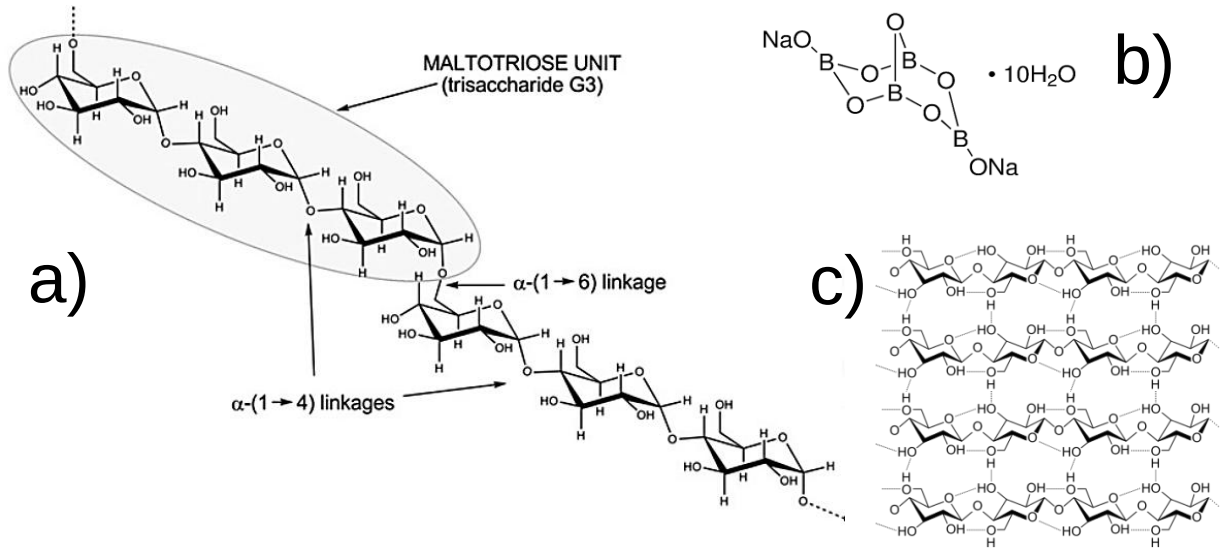
a)
MALTOTRIOSE UNIT
(trisaccharide G3)
α-(1→6) linkage
α-(1→4) linkages
b)
NaO
ONa
• 10H2O
c)

Figure 2

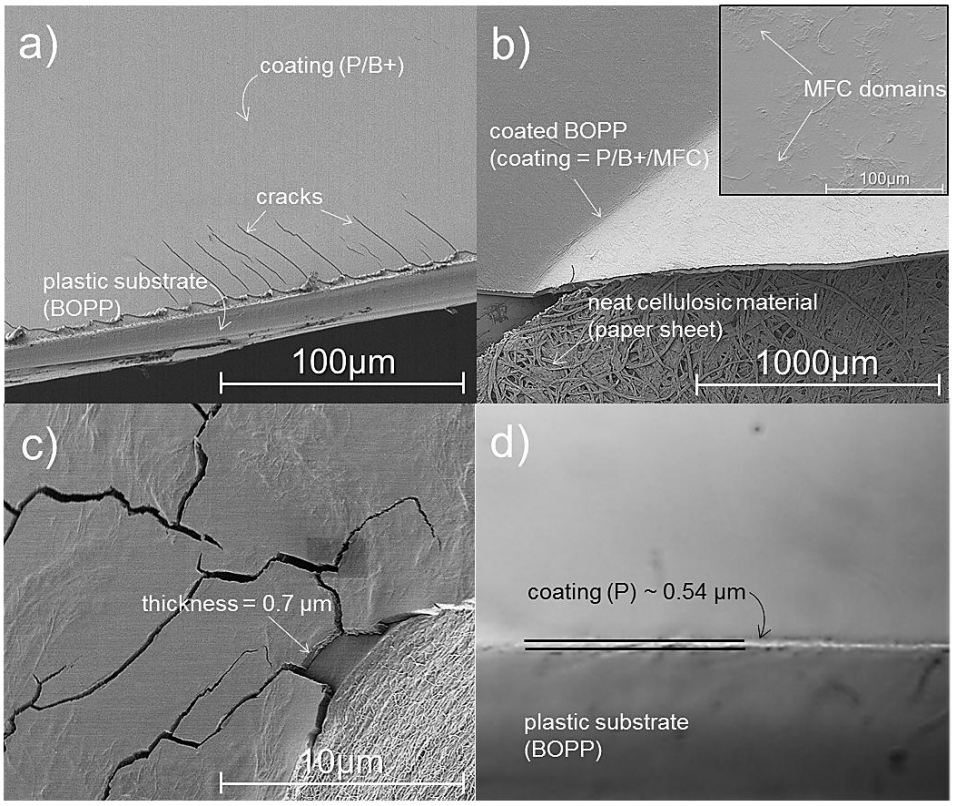
a)
coating (P/B+)
cracks
plastic substrate
(BOPP)
100µm
b)
MFC domains
100µm
coated BOPP
(coating = P/B+/MFC)
heat cellulosic material
(paper sheet)
1000µm
c)
thickness = 0.7 µm
10µm
d)
coating (P) ~ 0.54 µm
plastic substrate
(BOPP)

Figure 3

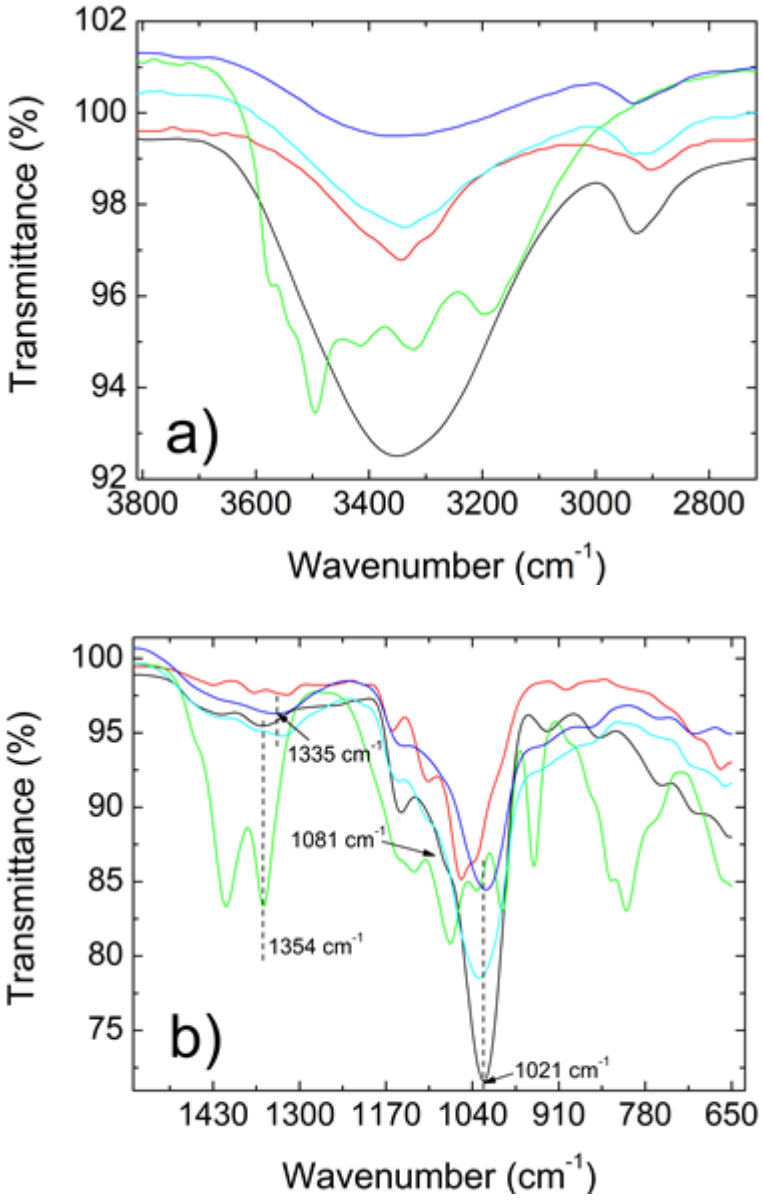
Transmittance (%)
102
100
98
96
94
92
a)
3800
3600
3400
3200
3000
2800
Wavenumber (cm-1)
Transmittance (%)
100
95
90
85
80
75
b)
1335 cm-1
1081 cm-1
1354 cm-1
1021 cm-1
1430
1300
1170
1040
910
780
650
Wavenumber (cm-1)

Figure S1

Microfibrillated cellulose and borax as mechanical, O_2-barrier, and surface–modulating agents of pullulan biocomposite coatings on BOPP

Carlo A. Cozzolino, Gaetano Campanella, Hasan Türe, Richard T. Olsson, Stefano Farris*

Supporting Information

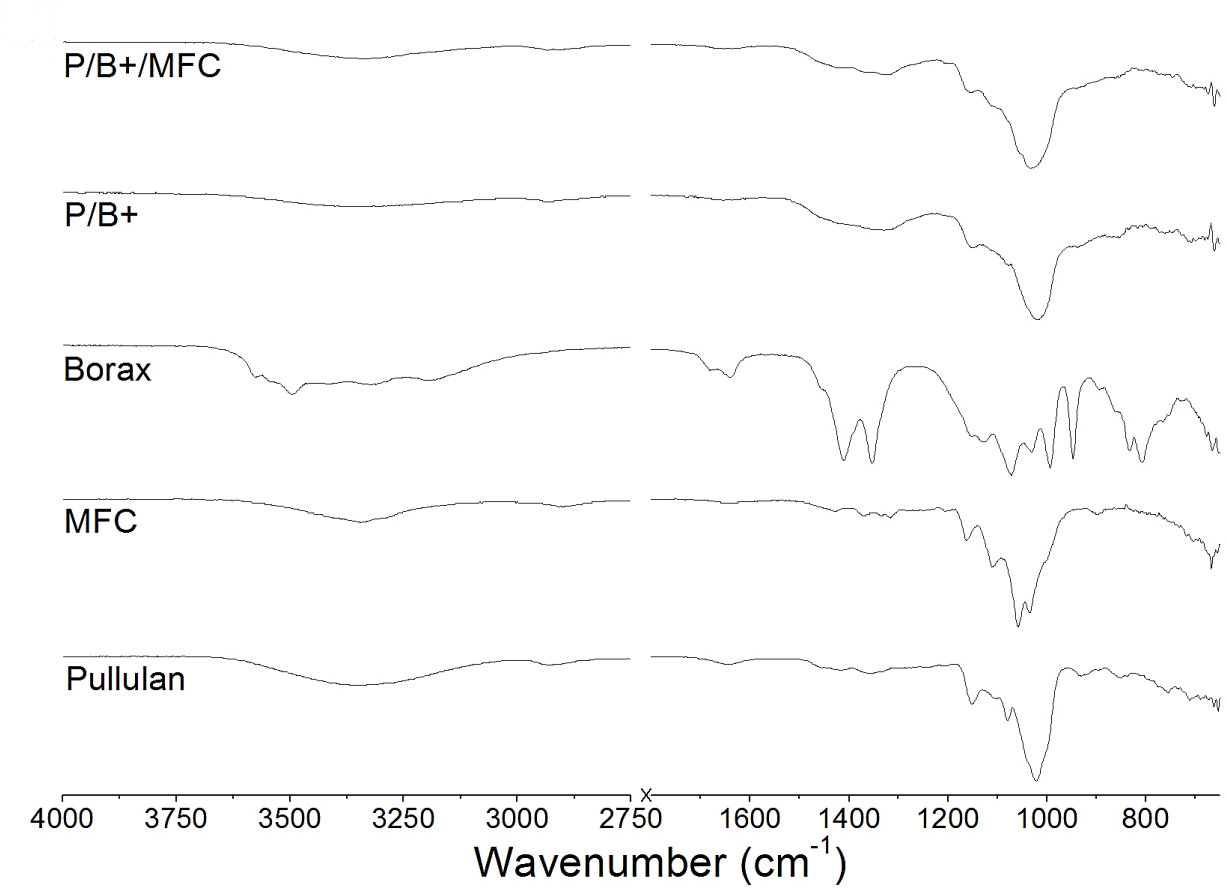

Figure S1. FTIR/UATR raw spectra of pullulan, microfibrillated cellulose (MFC), borax, and the composites P/B+ and P/B+/MFC